Efficient Depth Image Reconstruction using Accelerated Proximal Gradient Method

Mau Uyen Nguyen Thanh Tinh Dao Van Ha Tang
Faculty of Information Technology, Le Quy Don Technical University, Hanoi, Vietnam
Emails: nguyenitt2005@gmail.com, tinhdt@mta.edu.vn, hatv@lqdtu.edu.vn

***Abstract*—This paper presents an accelerated proximal gradient technique for depth image reconstruction from incomplete data samples. One of the most technical challenges in depth imaging is to estimate a depth image from sparse measurements obtained due to missing depth values or fast sensing. Recent advances in signal processing, i.e., compressive sensing (CS) allows the depth image to be reconstructed precisely from far reduced measurements provided that the image has sparse representations in proper bases. Inspired by the CS theory, this paper formulates the task of depth channel reconstruction as a sparsity-regularized least squares optimization problem. To solve this problem efficiently, an iterative algorithm based on the accelerated proximal gradient technique is developed, which not only speeds up the convergence rate, but also enhances the quality of depth image estimation. Several experiments are conducted and the results confirm the efficiency of the proposed approach.**

I. Introduction

Over the past two decades, depth sensing has witnessed increasing research interests due to its abilities to provide the depth channel information together with the conventional 2-D image of the desired scene. The capability of generating the depth channel image and thereby yielding the 3-D model of the desired scene is highly desirable in numerous applications, including autonomous driving, robot navigation, and augmented reality [1]–[3]. However, depth sensing technologies produce the depth channel images with prolonged data acquisition time and missing values despite recent developments in RGB-D cameras like Microsoft Kinect, Intel RealSense, and Google Tango. Thus, new approaches for fast data acquisition and efficient depth reconstruction are needed to enhance the efficiency and practicality of the depth sensing technology.

Techniques for recovering missing values of the depth channel image have been reported in several studies. Classic methods based on shapes were proposed in [1] and [2]. While the method in [1] used shading shapes, the technique in [2] exploited the defocusing shape to fill the missing pixels on the depth image. Other conventional approaches considered hand-tuned models and assumed the availability of the surface orientations [4], [5]. Image inpainting approaches have also introduced to depth estimate. The work in [6] enhanced depth image using region growing and bilateral filtering, whereas the approach in [7] used Kalman filter to smooth the depth map. However, these approaches require the availability of a color image of the scene, which prolongs data acquisition time. Furthermore, such existing methods are related to low-resolution depth map effects.

Recent approaches based on compressive sensing (CS) [8], [9] for depth estimate were proposed in [10], [11]. The emerging CS framework enables the depth image to be reconstructed precisely from incomplete pixels (measurements) by exploiting sparse structures of the depth channel image in proper bases. More importantly, CS enables the reconstruction and compression to be performed simultaneously, resulting in simple and cost-effective hardware sensing systems. In the sparsity-based technique, the task of depth reconstruction is posed as a sparse-regularized least squares (LS) optimization problem. To solve this problem, the study in [10] applied first-order subgradient method, while the alternating direction method of multipliers algorithm was used in [11]. These algorithms can be regarded as special instances of the proximal gradient (PG) method [12], [13]. The PG technique is able to solve non-smooth and large-scale optimization problems, but it typically needs a large number of iterations when high accuracy is required.

In this paper, motivated by the CS-based approaches, we develop an iterative algorithm based on the accelerated proximal gradient (APG) method to estimate the depth channel image. The main aim is to keep the splitting capability from the PG counterpart and more importantly to enhance the convergence rate and quality of depth image reconstruction. This goal is achieved mainly by employing a smart strategy of computing an auxiliary point used for gradient evaluation and estimate of the solution. APG evaluates the auxiliary point as a linear combination of the previous estimates of the solution, whereas the standard PG uses only the current estimate. As a result, APG integrates both the splitting and accelerating capabilities. Extensive experiments and analysis on depth data are conducted and the results show that the APG requires far fewer

978-1-5386-6113-0/18/$31.00 ©2018 IEEE

iterations to converge and achieves higher accuracy of depth image reconstruction in comparison with the PG counterpart.

The remainder of the paper is organized as follows. Section II introduces the depth sparse sensing model. Section III describes the proposed APG approach for depth image reconstruction from sparse measurements. Section IV presents the experimental results. Section V gives concluding remarks.

II. Depth sparse sensing model

Consider the depth map $\mathbf{Z} \in \mathbb{R}^{h \times w}$ of a scene acquired by an active disparity sensor. Ideally, the sensor produces $m = h \times w$ entries representing the depth values from the sensor to the surrounding obstacles. However, due to fast sensing or missing effects, only n ($n \ll m$) measurements are obtained. Let $\mathbf{z} \in \mathbb{R}^m$ denote the vector obtained by vectorizing the corresponding unknown image $\mathbf{Z}$. Let $\mathbf{y} \in \mathbb{R}^n$ be the known measurements. The relation between $\mathbf{y}$ and $\mathbf{Z}$ can be mathematically expressed as

$$\mathbf{y} = \mathbf{\Phi}\, \mathbf{z}, \tag{1}$$

where $\mathbf{\Phi} \in \mathbb{R}^{n \times m}$ is the sampling matrix representing the down-sampling protocol in CS operations or the linear operator modeling missing-valued effects.

The depth image $\mathbf{Z}$ typically comprises large homogenous regions of pixel values with only a few discontinuous at the transitions between those regions. This important property makes the depth image be much more sparse compared to natural images when representing in proper domains, such as wavelets [11], [14]. The sparsity associated with the wavelet transform can be interpreted by the fact that large homogeneous regions are compressively represented by only a small number of significant wavelet coefficients. Let $\mathbf{\Psi} \in \mathbb{R}^{m \times q}$ be the dictionary matrix containing in its columns q ($q \geq m$) wavelet bases. The sparse representation of image $\mathbf{z}$ can be mathematically modeled as

$$\mathbf{z} = \mathbf{\Psi}\, \mathbf{x}, \tag{2}$$

where $\mathbf{x} \in \mathbb{R}^q$ is a coefficient vector containing only s nonzero components, i.e., $s = \|\mathbf{x}\|_0$. For a sparse representation, s is significantly smaller than q ($s \ll q$). It is worth noting here that the ℓ_0-norm measures exactly the number of nonzero components of a vector or matrix, but in practice its counterpart, the ℓ_1-norm, is used to enforce the sparsity of the problem since it is a convex relaxation for the ℓ_0-norm [15].

From Eqs. (1) and (2), given the observation vector $\mathbf{y}$, the reconstruction of $\mathbf{x}$ can be formulated as an ℓ_1-regularized LS optimization problem:

$$\hat{\mathbf{x}} = \arg\min_{\mathbf{x}} f(\mathbf{x}) = \frac{1}{2}\|\mathbf{y} - \mathbf{A}\, \mathbf{x}\|_2^2 + \lambda\, \|\mathbf{x}\|_1, \tag{3}$$

where we have defined $\mathbf{A} = \mathbf{\Phi}\, \mathbf{\Psi}$ and λ is a positive parameter used to trade off between the error (LS) and the ℓ_1 penalty terms. Solving Problem (3) yields an estimate $\hat{\mathbf{x}}$, then an image $\hat{\mathbf{z}}$ is approximated using Eq. (2), i.e., $\hat{\mathbf{z}} = \mathbf{\Psi}\, \hat{\mathbf{x}}$. In this representation, $\mathbf{\Psi}$ can be constructed from any bases. However, this paper considers only wavelet bases for depth image representations. Now, the remaining task is to solve the ℓ_1-regularized LS optimization problem (3). We propose an iterative algorithm based on APG method presented in the next section.

III. APG Depth Reconstruction

This section presents an APG-based algorithm to solve the ℓ_1-regularized LS problem in (3). Before presenting the APG method, it is convenient to describe the original PG technique for solving a generic minimization problem with a composite objective function.

A. Proximal gradient method

Consider a general case of minimizing a composite objective function:

$$\min_{\mathbf{x}} f(\mathbf{x}) = g(\mathbf{x}) + \lambda\, h(\mathbf{x}), \tag{4}$$

where $g(\mathbf{x})$ is convex, differentiable, and smooth, e.g., the quadratic term in (3) and $h(\mathbf{x})$ is convex but not necessary smooth, e.g., the ℓ_1-norm term in (3). In general, it is hard or complicated to deal with Problem (4) directly. One common strategy is to split the objective function using a *proximal gradient iterative technique*. Let $\mathbf{x}_k$ denote an estimate of the solution at the k-th iteration. Then, the next estimate of the minimizer is obtained by solving:

$$\mathbf{x}_{k+1} = \arg\min_{\mathbf{x}} \frac{1}{2}\, \|\mathbf{a}_k - \mathbf{x}\|_2^2 + \lambda\alpha\, h(\mathbf{x}), \tag{5}$$

where

$$\mathbf{a}_k = \mathbf{x}_k - \alpha \nabla g(\mathbf{x}_k). \tag{6}$$

Here, $\nabla g(\mathbf{x}_k)$ denotes the gradient of $g(\mathbf{x})$ evaluated at the current estimate $\mathbf{x}_k$. When ∇g is a Lipschitz continuous function with constant C, this method converges if $\alpha \in (0,\ 1/C]$. This generic optimization technique and its convergence guarantees have been widely used to solve the minimization problem (4) under different names: proximal gradient method [12], thresholded Landweber iteration [16], iterative shrinkage/thresholding [17], or separable approximation [18].

The iterative technique in (5)–(6) can be used to solve Problem (3) directly. Let $\mathbf{x}_k$ denote an estimate of the wavelet coefficient vector at the k-th iteration, Problem (3) can be minimized iteratively:

$$\mathbf{x}_{k+1} = \arg\min_{\mathbf{x}} \frac{1}{2}\, \|\mathbf{a}_k - \mathbf{x}\|_2^2 + \lambda\alpha\, \|\mathbf{x}\|_1, \tag{7}$$

where the auxiliary $\mathbf{a}_k$ is defined as

$$\mathbf{a}_k = \mathbf{x}_k - \alpha\, \mathbf{A}^T\, (\mathbf{A}\, \mathbf{x}_k - \mathbf{y}). \tag{8}$$

A typical condition ensuring convergence of $\{\mathbf{x}_k\}$ to a minimizer of (3) is to require that $\alpha \in (0, 1/\|\mathbf{A}\|_2^2]$. Hereafter, $\|\mathbf{A}\|_2$ denotes the spectral norm of matrix $\mathbf{A}$ (i.e., maximum singular value of the matrix). Now the problem is to solve Subproblem (7), which admits a closed-form solution that will be presented in Subsection III-C.

Obviously, the PG technique is useful for solving the ℓ_1-regularized LS optimization problem. The computation effort at each iteration involves only simple matrix computation for the gradient evaluation in (8), followed by solving a subproblem with a closed-form solution. This makes the iterative PG method computationally efficient, and very suitable for solving the large-scale depth reconstruction problem. However, the PG technique converges slowly with a worst-case complexity result of $\mathcal{O}(1/k)$. Detail proofs are described in the general framework of proximal forward-backward splitting [12], [19], special PG instances of iterative shrinkage technique [20], and projected gradient [21]. To enhance the efficiency and practicality of depth imaging, the next subsection introduces an accelerated scheme that holds the computational efficiency at each iteration of the standard PG, but enhances the global rate of convergence considerably.

B. Accelerated proximal gradient method

To accelerate the convergence rate, it is crucial to modify the computation for the next estimate $\mathbf{x}_{k+1}$ in the original PG scheme presented in Eqs. (5) and (6). Here, the next estimate of the solution $\mathbf{x}_{k+1}$ is obtained using an auxiliary point $\mathbf{a}_k$, which is computed using only the previous estimate $\mathbf{x}_k$. In [22], Nesterov showed that in the smooth case, i.e., $h(\mathbf{x}) \equiv 0$, the global rate of convergence for Problem (4) can be improved to $\mathcal{O}(1/k^2)$ by choosing a smart auxiliary point that is easy to compute. In particular, the point $\mathbf{a}_k$ should be evaluated from another auxiliary point $\mathbf{u}_k$ which is chosen from a linear combination of the previous estimates $\mathbf{x}_k$ and $\mathbf{x}_{k-1}$:

$$\mathbf{u}_k = \mathbf{x}_k + \frac{t_{k-1} - 1}{t_k}(\mathbf{x}_k - \mathbf{x}_{k-1}), \tag{9}$$

$$\mathbf{a}_k = \mathbf{u}_k - \alpha \nabla g(\mathbf{u}_k), \tag{10}$$

for a sequence $\{t_k\}$ satisfying

$$t_k^2 - t_k \leq t_{k-1}^2. \tag{11}$$

In the non-smooth case, i.e., $h(\mathbf{x}) \not\equiv 0$, Beck and Teboulle in [23] and Nesterov in [24] have proved that the updating schemes in Eqs. (5), (9), and (10) are valid to ensure the convergence rate of $\mathcal{O}(1/k^2)$.

Using the APG scheme, the ℓ_1-regularized LS depth imaging problem in (3) can be solved effectively incorporating both splitting and accelerating features. After $\mathbf{u}_k$ is defined as in (9), the auxiliary point $\mathbf{a}_k$ is obtained in a similar manner as in the original PG scheme given by (8):

$$\mathbf{a}_k = \mathbf{u}_k - \alpha\, \mathbf{A}^T\, (\mathbf{A}\, \mathbf{u}_k - \mathbf{y}). \tag{12}$$

Now the remaining task is to solve Subproblem (7). Detailed steps are presented in the following subsection.

C. Solving subproblem

This subsection presents an efficient technique to solve Subproblem (7). This problem is convex, which can be recast as a semidefinite program and solved based on interior-point methods. This technique, however, is slow and problematic when the size of $\mathbf{x}$ is large (e.g., $q > 10,000$) because it needs to solve huge systems of linear equations to compute the Newton direction. In this paper, this minimization problem is solved efficiently using the *soft-thresholding/shrinkage* technique, which provides a closed-form solution. Let us consider the following theorem [20], [25]:

Theorem 1: For each $\tau \geq 0$ and $\mathbf{a} \in \mathbb{R}^q$, the shrinkage $\mathcal{T}(\mathbf{a}, \tau)$ obeys

$$\mathcal{T}(\mathbf{a}, \tau) = \arg\min_{\mathbf{x}} \frac{1}{2} \|\mathbf{a} - \mathbf{x}\|_2^2 + \tau \|\mathbf{x}\|_1 . \tag{13}$$

Theorem 1 is proved based on the concept of proximal gradient operator of convex functions (here the ℓ_1-norm). In (13), the soft-thresholding operator $\mathcal{T}(\mathbf{a}, \tau)$ is a nonlinear function which applies a soft-thresholding at level τ to the entries of the input vector $\mathbf{a}$:

$$\mathcal{T}(a, \tau) = \mathrm{sgn}(a) \max(|a| - \tau, 0) = \frac{a}{|a|} \max(|a| - \tau, 0). \tag{14}$$

Note that when applied to vectors or matrices, the soft-thresholding operator $\mathcal{T}(\cdot, \tau)$ performs entrywise. Using Theorem 1, the solution to Subproblem (7) is given by

$$\mathbf{x}_{k+1} = \mathcal{T}(\mathbf{a}_k, \lambda\, \alpha). \tag{15}$$

In summary, the iterative steps of the original and accelerated PG algorithms for solving depth imaging Problem (3) are provided in Table I and Table II, respectively. The two algorithms take an input set of the data measurements $\mathbf{y}$, the parameters α, λ, and a predefined tolerance tol. The parameter α can be regarded as a gradient stepsize and should be set to the largest possible values for fast convergence, whereas the regularization parameter λ is problem-dependent and needs to be tuned appropriately. Further

discussion on selecting suitable parameters is given in experimental section IV-A. In the processing steps, the two algorithms obviously perform two major tasks: gradient evaluation (Step 2) and depth image estimate (Step 3) by soft-thresholding.

The main difference between the two algorithms is the computation of the auxiliary points for performing gradient splitting at Step 2. In the original PG, the auxiliary point is computed using only the current estimate of $\mathbf{x}_k$, whereas in the APG scheme, the auxiliary variable is obtained from $\mathbf{u}_k$ evaluated as a linear combination of the two previous estimates $\mathbf{x}_k$ and $\mathbf{x}_{k-1}$. By doing so, the computational effort in the APG keeps as simple as the original PG, but accelerates the global rate of convergence. For fastest convergence, the sequence $\{t_k\}$ should increase as fast as possible and here, the update $t_{k+1} \leftarrow \frac{1+\sqrt{4t_k^2+1}}{2}$ is chosen by solving (11) with the inequality replaced by equality. The algorithms stop when they converge to a global optimum ($f(\mathbf{x})$ is a convex function). In implementation, the algorithms terminate if the relative change of the objective function is negligible (see Step 4). After that, the column vector $\mathbf{z}$ is reshaped into a 2-D map representing the reconstructed depth image.

TABLE I
ALGORITHM 1: PG-BASED ITERATIVE ESTIMATION OF DEPTH IMAGE.

1) Initialize $\mathbf{x}_0 \leftarrow \mathbf{0}$, $\mathbf{z}_0 \leftarrow \mathbf{\Psi}\,\mathbf{x}_0$, and $k \leftarrow 0$.

2) Perform gradient splitting using (6):

$$\mathbf{a}_k \leftarrow \mathbf{x}_k - \alpha\,\mathbf{A}^T\,(\mathbf{A}\,\mathbf{x}_k - \mathbf{y}).$$

3) Estimate depth image using (15) and (2):

$$\mathbf{x}_{k+1} \leftarrow \mathcal{T}(\mathbf{a}_k, \lambda\,\alpha),$$
$$\mathbf{z}_{k+1} \leftarrow \mathbf{\Psi}\,\mathbf{x}_{k+1}.$$

4) Evaluate the cost function $f(\mathbf{x}_{k+1})$ using (3) and

if $\frac{|f(\mathbf{x}_{k+1})-f(\mathbf{x}_k)|}{|f(\mathbf{x}_k)|} < \mathrm{tol}$ then terminate the algorithm,

otherwise increment $k \leftarrow k+1$ and go to Step 2.

IV. EXPERIMENTAL RESULTS

In this section, we present the experimental results on real depth imaging data. Subsection IV-A describes the experiment setup. Subsection IV-B provides results and performance analysis for several imaging methods.

A. Experimental setup

The proposed APG algorithm is evaluated based on the Middlebury Stereo Dataset [26], where the ground truth disparity maps are available. Using the same input

TABLE II
ALGORITHM 2: APG-BASED ITERATIVE ESTIMATION OF DEPTH IMAGE.

1) Initialize $\mathbf{x}_1 = \mathbf{x}_0 \leftarrow \mathbf{0}$, $k \leftarrow 1$, $t_1 = t_0 \leftarrow 1$.

2) Perform gradient splitting using (9) and (12):

$$\mathbf{u}_k \leftarrow \mathbf{x}_k + \tfrac{t_{k-1}-1}{t_k}(\mathbf{x}_k - \mathbf{x}_{k-1}),,$$

$$\mathbf{a}_k \leftarrow \mathbf{u}_k - \alpha\,\mathbf{A}^T\,(\mathbf{A}\,\mathbf{u}_k - \mathbf{y}).$$

3) Estimate depth image using (15) and (2):

$$\mathbf{x}_{k+1} \leftarrow \mathcal{T}(\mathbf{a}_k, \lambda\,\alpha),$$
$$\mathbf{z}_{k+1} \leftarrow \mathbf{\Psi}\,\mathbf{x}_{k+1}.$$

4) Evaluate the cost function $f(\mathbf{x}_{k+1})$ using (3) and

if $\frac{|f(\mathbf{x}_{k+1})-f(\mathbf{x}_k)|}{|f(\mathbf{x}_k)|} < \mathrm{tol}$ then terminate the algorithm,

otherwise $t_{k+1} \leftarrow \frac{1+\sqrt{4t_k^2+1}}{2}$, $k \leftarrow k+1$, go to Step 2.

depth data, we aim to compare the performances of the PG and APG in terms of reconstruction quality and convergence rate. To quantify the quality of depth image reconstruction, the peak signal-to-noise ratio (PSNR) is used (in dB):

$$\mathrm{PSNR} = 10\log_{10}\left(\frac{I_{\mathrm{peak}}^2}{\mathrm{MSE}}\right), \tag{16}$$

where I_{peak} is the peak intensity of reconstructed image I, and MSE is the mean-square-error between the reconstructed image I and the ground-truth image I_g defined as

$$\mathrm{MSE} = \frac{1}{h \times w}\sum_{i=1}^{h}\sum_{j=1}^{w}|I(i,j) - I_g(i,j)|^2. \tag{17}$$

The dictionary transform $\mathbf{\Psi}$ is constructed from 2-D symmetric wavelets with symmetric boundary treatments using lifting implementation. The parameters for both PG and APG-based algorithms are chosen as follows. The parameter α (gradient stepsize) is selected as $\alpha = 1/\|\mathbf{A}\|_2^2$ for accelerated convergence. The regularization parameter λ is set to $\lambda = 0.03$. The algorithm converges if the relative change of the objective function is smaller than $\mathrm{tol} = 10^{-5}$ (see Step 4).

B. Experimental results

In the first experiment, we aim to evaluate the performances of the APG and PG-based algorithms under CS contexts where the compressive sensor acquires only far reduced measurements for imaging. In doing so, only 50% measurements of the total

pixels are randomly sampled from a ground-truth depth image of an art, shown in Fig. 1(a). Because only 50% measurements are acquired, the depth image is corrupted as shown in Fig. 1(b). Using the 50% data measurements, the depth images reconstructed by the PG and APG-based algorithms are presented in Figs. 1(c) and (d), respectively. Both PG and APG recover the depth image well, but APG yields a higher quality image (PSNR=31.10 dB) than does the PG method (PSNR=28.56 dB).

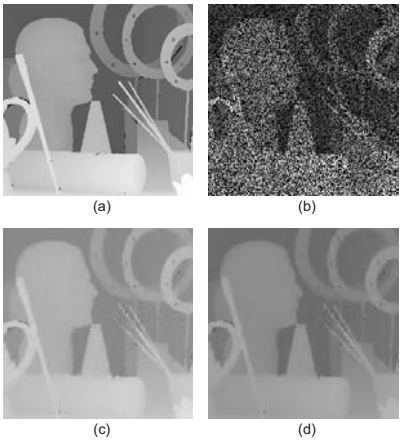

Fig. 1. Depth image reconstructed using different sparsity-based CS methods: (a) Ground-truth depth image of art, (b) Corrupted depth image with only 50% data measurements (PSNR=7.02 dB), (c) reconstructed image by PG [10], [11] (PSNR=28.56 dB), and (d) reconstructed image by the proposed APG (PSNR=31.10 dB).

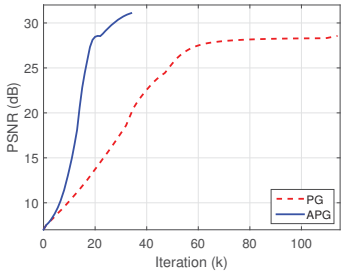

Fig. 2. PSNRs of the depth image reconstructed by PG (dashed line) and APG (solid line) recorded during the minimization using 50% of total measurements. At initialization, PSNRs by both algorithms are the same, at 7.02 dB. The proposed APG converges after 35 iterations and achieves an PSNR of 31.10 dB, whereas PG converges after 115 iterations and obtains an PSNR of 28.56 dB.

For further insights into PG and APG algorithms, we record the PSNR values of the estimated image and the cost function during the loop for depth image reconstruction. Fig. 2 shows the PSNRs of the images estimated by PG and APG during minimization. It can be observed that APG requires far fewer number of iterations to achieve high quality of depth image

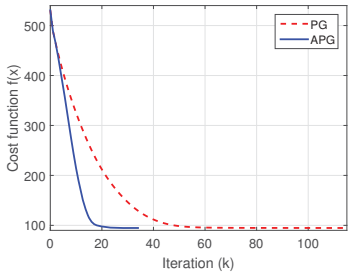

Fig. 3. Objective function values $f(\mathbf{x})$ recorded during minimization by PG (dashed line) and APG (solid line) using 50% of total measurements. At initialization, the values of the cost function is 530.72 for both algorithms. The cost function by the proposed APG reaches 94.75 after 35 iterations, whereas the cost function by PG decreases to 94.77 after 115 iterations.

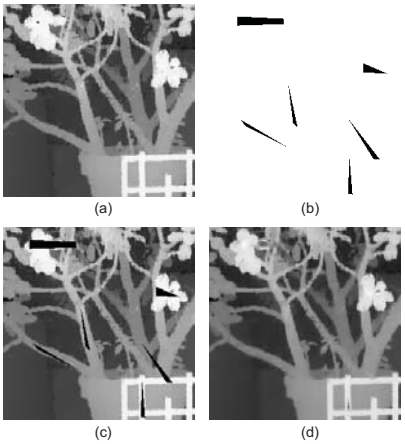

Fig. 4. Depth image reconstructed using sparsity-based APG method: (a) Ground-truth depth image of an jade plant, (b) A mask representing missing values (black pixels), (c) corresponding depth image with missing values (PSNR=18.25 dB), and (d) reconstructed image by APG (PSNR=31.37 dB).

reconstruction. For example, to reach PSNR=28 dB, APG needs only 20 iterations whereas PG requires 60 iterations. Fig. 3 depicts the objective function during the loop. Obviously, both algorithms converge, but the converange rate of APG is much faster than that of PG counterpart.

In the second experiment, we aim to test the proposed APG method for recovering depth images with missing values. The missing-value depth image is generated by using a mask. The ground-truth depth image of a jade plant and the mask are shown in Figs. 4(a) and (b), respectively. Due to missing values, the image is distorted as demonstrated in Fig. 4(c). Using the available pixel measurements, the image reconstructed by APG method is presented in Fig. 4(d), where the missing pixels are restored.

V. Conclusion

This paper presented an accelerated proximal gradient method for depth image reconstruction from sparse measurements. Compressive depth sensing yields corrupted images with missing values. The APG approach allows a high-quality image to be reconstructed from the CS measurements via solving a sparse-regularized LS optimization problem. By incorporating both splitting and accelerating features, APG produces accurate image reconstruction while speeds up global rate of convergence. Experimental results are conducted and the results show that the proposed APG approach enhances the quality of image reconstruction and convergence rate, especially in comparison with its PG counterpart. Future work will investigate different sparse representation dictionaries, including dictionary learning, for further enhancing the performance of the APG model.

References

[1] R. Zhang, P.-S. Tsai, J. E. Cryer, and M. Shah, "Shape from shading: A survey," *IEEE Trans. Pattern Anal. and Machine Intell.*, vol. 21, no. 8, pp. 690–706, 1999.

[2] S. Suwajanakorn, C. Hernandez, and S. M. Seitz, "Depth from focus with your mobile phone," in *IEEE Conf. Comput. Vision and Pattern Recognition*, 2015, pp. 3497–3506.

[3] W. Chen, Z. Fu, D. Yang, and J. Deng, "Single-image depth perception in the wild," in *Advances in Neural Inform. Process. Systems*, 2016, pp. 730–738.

[4] A. Saxena, S. H. Chung, and A. Y. Ng, "Learning depth from single monocular images," in *Advances in Neural Inform. Process. Systems*, 2006, pp. 1161–1168.

[5] M. Sun, A. Y. Ng, and A. Saxena, "Make3D: Learning 3D scene structure from a single still image," *IEEE Trans. Pattern Analysis and Machine Intell.*, vol. 31, no. 5, pp. 824–840, 2009.

[6] L. Chen, H. Lin, and S. Li, "Depth image enhancement for kinect using region growing and bilateral filter," in *IEEE Int. Conf. Pattern Recognition*, 2012, pp. 3070–3073.

[7] M. Camplani and L. Salgado, "Adaptive spatio-temporal filter for low-cost camera depth maps," in *IEEE Int. Conf. Emerging Signal Process. Appl.*, 2012, pp. 33–36.

[8] D. L. Donoho, "Compressed sensing," *IEEE Trans. Inform. Theory*, vol. 52, no. 4, pp. 1289–1306, Apr. 2006.

[9] E. J. Candes, J. Romberg, and T. Tao, "Stable signal recovery from incomplete and inaccurate measurements," *Comm. on Pure and Applied Math.*, vol. 59, no. 8, pp. 1207–1223, Aug. 2006.

[10] S. Hawe, M. Kleinsteuber, and K. Diepold, "Dense disparity maps from sparse disparity measurements," in *IEEE Int. Conf. Comput. Vision*, 2011, pp. 2126–2133.

[11] L.-K. Liu, S. H. Chan, and T. Q. Nguyen, "Depth reconstruction from sparse samples: Representation, algorithm, and sampling," *IEEE Trans. Image Process.*, vol. 24, no. 6, pp. 1983–1996, 2015.

[12] P. L. Combettes and V. R. Wajs, "Signal recovery by proximal forward-backward splitting," *SIAM J. Multiscale Modeling Simulation*, vol. 4, no. 4, pp. 1168–1200, Nov. 2006.

[13] N. Parikh and S. Boyd, "Proximal algorithms," in *Foundations and Trends in Optimization*, vol. 1, no. 3. Now Publishers Inc, Nov. 2013, pp. 123–231.

[14] S. Mallat, *A Wavelet Tour of Signal Processing, Third Edition: The Sparse Way*. Academic Press, Inc. Orlando, FL, USA, 2008.

[15] O. Scherzer, *Handbook of Mathematical Methods in Imaging*. Springer Science, New York, USA, 2011.

[16] C. Vonesch and M. Unser, "A fast thresholded Landweber algorithm for wavelet-regularized multidimensional deconvolution," *IEEE Trans. Image Process.*, vol. 17, no. 4, pp. 539–549, April 2008.

[17] J. M. Bioucas-Dias and M. A. T. Figueiredo, "A new TwIST: two-step iterative shrinkage/thresholding algorithms for image restoration," *IEEE Trans. Image Process.*, vol. 16, no. 12, pp. 2992–3004, Dec. 2007.

[18] S. J. Wright, R. D. Nowak, and M. A. T. Figueiredo, "Sparse reconstruction by separable approximation," *IEEE Trans. Signal Process.*, vol. 57, no. 7, pp. 2479–2493, July 2009.

[19] P. L. Combettes and J. Pesquet, "Proximal splitting methods in signal processing," in *Fixed-Point Algorithms for Inverse Problems in Science and Engineering*. H. Bauschke, R. Burachik, P. L. Combettes, V. Elser, D. Luke, H. Wolkowicz (eds), Springer, New York, NY, 2011, pp. 185–212.

[20] I. Daubechies, M. Defrise, and C. D. Mol, "An iterative thresholding algorithm for linear inverse problems with a sparsity constraint," *Comm. Pure and Applied Math.*, vol. 57, no. 11, pp. 1413–1457, Nov. 2004.

[21] M. A. T. Figueiredo, R. D. Nowak, and S. J. Wright, "Gradient projection for sparse reconstruction: Application to compressed sensing and other inverse problems," *IEEE J. Selected Topics in Signal Process.*, vol. 1, no. 4, pp. 586–597, 2007.

[22] Y. E. Nesterov, "A method of solving a convex programming problem with convergence rate $\mathcal{O}(1/k^2)$," *Soviet Math. Doklady*, vol. 27, no. 2, pp. 372–376, 1983.

[23] A. Beck and M. Teboulle, "A fast iterative shrinkage-thresholding algorithm for linear inverse problems," *SIAM J. Imaging Sciences*, vol. 2, no. 1, pp. 183–202, March 2009.

[24] Y. E. Nesterov, "Gradient methods for minimizing composite functions," *Mathematical Programming*, vol. 140, no. 1, pp. 125–161, Aug. 2013.

[25] D. L. Donoho, "De-noising by soft-thresholding," *IEEE Trans. Inf. Theory*, vol. 41, no. 3, pp. 613–627, May 1995.

[26] D. Scharstein, H. Hirschmller, Y. Kitajima, G. Krathwohl, N. Nesic, X. Wang, and P. Westling, "High-resolution stereo datasets with subpixel-accurate ground truth," in *German Conf. Pattern Recognition*, Sep. 2014, vol. 8753, pp. 31–42.